Tomography with grating interferometers at low-brilliance sources

Timm Weitkamp[a*], Christian David[b], Christian Kottler[b], Oliver Bunk[c], and Franz Pfeiffer[c]

[a]Institut für Synchrotronstrahlung / ANKA Light Source,
Forschungszentrum Karlsruhe, Postfach 36 40, 76021 Karlsruhe, Germany

[b]Laboratory for Micro- And Nanotechnology, Paul Scherrer Institut, 5232 Villigen PSI, Switzerland

[c]Swiss Light Source, Paul Scherrer Institut, 5232 Villigen PSI, Switzerland

ABSTRACT

The coherence requirements for efficient operation of an X-ray grating interferometer are discussed. It is shown how a Talbot–Lau geometry, in which an array of equidistant secondary sources is used, can be used to decouple fringe visibility in the interferometer (and thus, its efficiency) from the total size of the X-ray source. This principle can be used for phase-contrast radiography and tomography with sources of low brilliance, such as X-ray tubes.

Keywords: X-ray tomography, phase contrast, coherence, Talbot interferometer, Talbot–Lau interferometer, phase-stepping interferometry, synchrotron radiation, microtomography, phase reconstruction

1. INTRODUCTION

Grating interferometry with hard X rays is a phase-sensitive radiography method whose main advantages over existing X-ray phase contrast methods are, firstly, the potential to realize fields of view large enough for such application fields as industrial non-destructive testing, security screening, and medical imaging, and, secondly, the possibility to efficiently use curved wavefronts and low-brilliance sources. The signal obtained is essentially the first derivative of the wavefront phase profile along a given transverse direction, from which a quantitative phase profile can be reconstructed by integration. The amplitude profile is also accessible from the interferogram data. When combined with a tomographic scan, this makes it possible to reconstruct the three-dimensional distribution of X-ray refractive index in the sample, as well as the distribution of absorption coefficient commonly obtained in absorption tomography.

The main objective of this paper is to discuss in some detail the requirements on the spatial, or transverse, coherence properties of the illuminating radiation in X-ray grating interferometers, and to show how the use of a structured source can make the use of low-brilliance installations with a grating interferometer efficient.

2. TALBOT INTERFEROMETER

X-ray grating interferometers, also referred to as *shearing* or *Talbot* interferometers, today generally use two linear transmission gratings to detect the wavefront phase gradient. The transmission gratings are thin slabs placed in the beam perpendicular to the optical axis, and containing periodical line structures that absorb X rays and/or shift their phase (Fig. 1).

The first of these two gratings, which we denote here by G1, induces a periodic spatial modulation in the amplitude and/or the phase of the X-ray wavefront. This makes the grating a diffractive element that can be interpreted as a *beam splitter*, even though the angular separation of the two beams is so small that the beams are not spatially separated, but rather interfere with one another. The wavefront modulation induced by G1 can be observed in the form of fringe patterns in the X-ray intensity distribution at suitable positions downstream of the grating. Distortions of the incident wavefront, where present, lead to distortions of the modulation. By detecting the ensuing irregularities in the fringe positions, it is possible to reconstruct the wavefront shape and, thus, the wavefront phase profile.

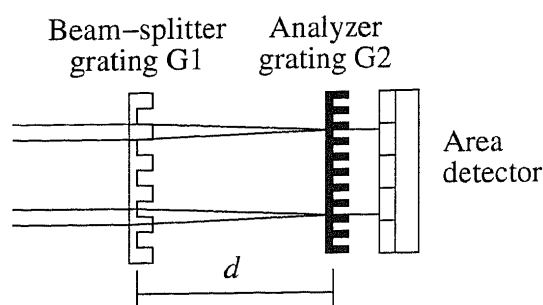*E-mail: timm.weitkamp@iss.fzk.de; Telephone: +49 72 47 82 68 64

Figure 1: Schematic setup of a Talbot interferometer for X rays.

However, the fringes are usually too closely spaced for their positions to be registered directly on a detector. It is therefore necessary to place a second grating, G2, with strongly absorbing lines, close to the detector. This grating acts as an *analyzer* in that it transforms fringe positions into intensity values. These can then be recorded with a detector. The detector may have a pixel size much larger than the periodicity of the fringes.

This scheme was first proposed in 2002 in a paper reporting the experimental realization of a slightly more complex precursor setup.[1] It was experimentally demonstrated in the following year[2] and has since been used for phase radiography and tomography and for X-ray optics characterization.[3-10] The separation of the phase signal from the absorption information is best performed with a phase-stepping method,[7] but moiré techniques can also be applied.[6] They have the advantage of simpler measurement and a smaller amount of raw data, albeit at much reduced spatial resolution.
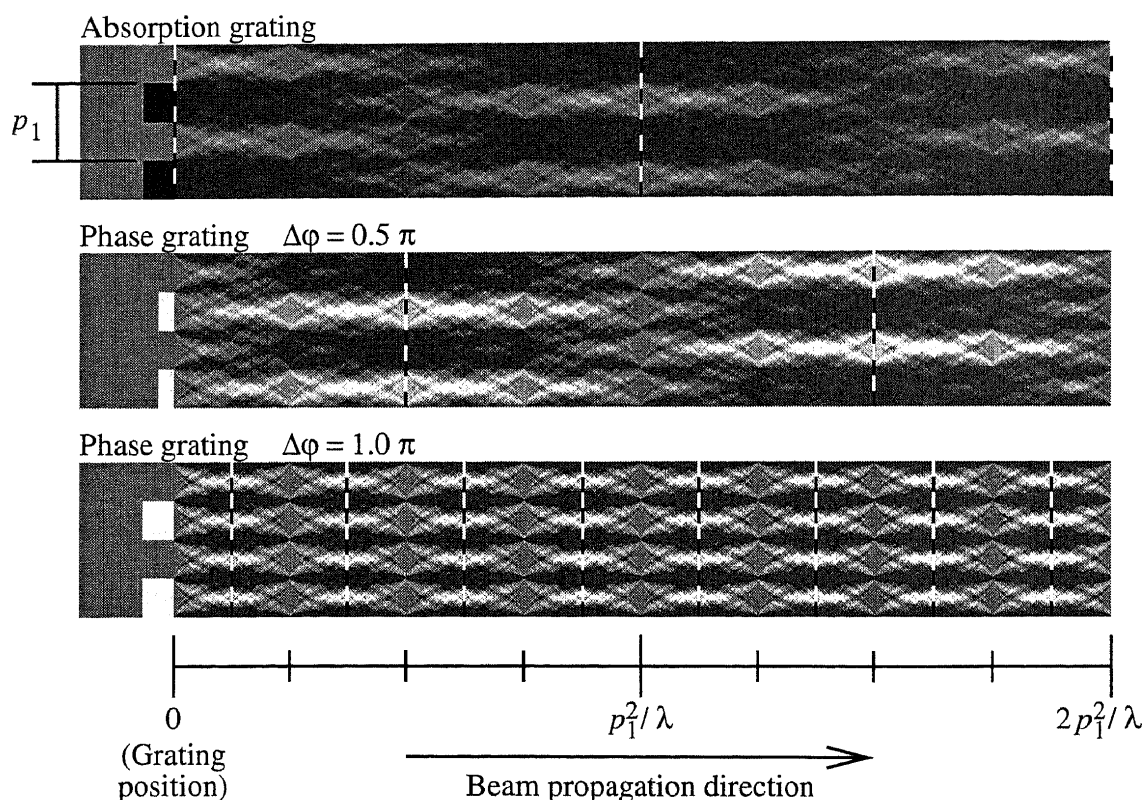

Figure 2: Intensity distribution for an incident coherent plane wave behind a grating of period p_1 that acts as a beam splitter. The three panels differ only in the optical properties of the grating. *Top:* amplitude grating with completely absorbing lines. *Center:* phase grating (zero absorption) with lines shifting the X-ray phase by 0.5π. *Bottom:* phase grating with lines shifting the X-ray phase by 1.0π. In all three panels, the positions of maximum contrast are indicated by black-and-white dashed lines.

While the analyzer grating, G2, must be an amplitude grating because its function is that of a transmission mask, the beam splitter grating, G1, can be a phase grating or an absorption grating, since both will lead to interference fringe patterns through the Talbot self-imaging effect. It is preferable to use a phase grating, i. e., a grating with negligible absorption, for the simple reason of photon efficiency. When using a phase grating, optimum visibility (and, thus, efficiency of the setup) is obtained when the grating material and thickness are chosen in such a way that the phase shift undergone by X rays passing through the grating lines is either $\pi/2$ or π.

The difference between these three different types of gratings (amplitude grating, quarter-wavelength phase grating, and half-wavelength phase grating) in terms of the intensity distribution downstream of the grating is shown in Fig. 2. All three cases have been experimentally realized in the different setups reported so far. As illustrated in Fig. 2, the Talbot distances, i. e., the positions along the optical axis at which the intensity fringe contrast takes a maximum or minimum, are, for an incident plane wave,

$$D_n = \frac{1}{\eta^2} \frac{np_1^2}{2\lambda} \quad (n = 0, 1, 2, \ldots) \tag{1}$$

Here, p_1 is the period of the beam-splitter grating G1. The integer number $n = 0, 1, 2, \ldots$ is called the *Talbot order*. The fringes from a phase grating will always have maximum contrast at odd Talbot orders ($n = 1, 3, 5, \ldots$), while an amplitude grating will produce maximum contrast at even Talbot orders ($n = 0, 2, 4, \ldots$).

The factor η reflects the interesting fact that, depending on the optical properties of the beam splitter G1, the fringe period is different:

$$\eta = \begin{cases} 1 & \text{if G1 is a } \pi/2\text{-shifting phase grating or an amplitude grating,} \\ 2 & \text{if G1 is a } \pi\text{-shifting phase grating,} \end{cases} \tag{2}$$

$$\tag{3}$$

and therefore, for an incident plane wave,

$$\begin{aligned} p_2 &= p_1 \quad (\pi/2\text{-shifting phase grating, amplitude grating}), \\ p_2 &= p_1/2 \quad (\pi\text{-shifting phase grating}). \end{aligned} \tag{4}$$

Note also that for the π-shifting (half-wavelength) phase grating, unlike for the two others, there is no reversal of the contrast occurring from one contrast maximum position along the optical axis to the next.

If the beam splitter is not illuminated by a plane wave, but by a spherical wave from a source at distance L, the Talbot distances are shifted and become

$$d_n = \frac{LD_n}{L - D_n} \overset{(Eq.1)}{=} \frac{L}{2\eta^2\lambda L/(np_1^2) - 1}, \tag{5}$$

and the fringe spacing at the Talbot distance d_n is stretched by a factor

$$M = \frac{L + d_n}{L} = \frac{L}{L - D_n} = 1 + \frac{d_n}{L} = \frac{d_n}{D_n}. \tag{6}$$

Here, as in Eq. 1, D_n denotes the Talbot distances for a plane wave, whereas d_n denotes those for a spherical wave with radius of curvature L. The fringe spacing and the period p_2 of the analyzer grating are therefore, in the case of a spherical wave,

$$p_2 = \frac{Mp_1}{\eta} \overset{(Eq.6)}{=} \frac{p_1}{\eta} \times \left(1 + \frac{d_n}{L}\right). \tag{7}$$

3. COHERENCE REQUIREMENTS

In this section, we discuss the coherence properties of the illuminating radiation that are required to obtain fringes with a given visibility. The visibility of the fringes is the most important figure of merit for the efficiency of the interferometer.

Concerning longitudinal coherence, or monochromaticity, it has been shown elsewhere[7, 10] how a deviation of the X-ray wavelength from its design value affects fringe contrast, and that an approximate expression for the monochromaticity required to maintain good contrast is[7]

$$\frac{\lambda_0}{\Delta\lambda} \gtrsim n, \tag{8}$$

where λ_0 is the design wavelength of the instrument, $\Delta\lambda$ the width of the wavelength distribution around λ_0, and n the Talbot order from Eq. 1. Equation 8 implies that a grating interferometer can be operated with very polychromatic radiation, which is one of the major assets of this type of device.
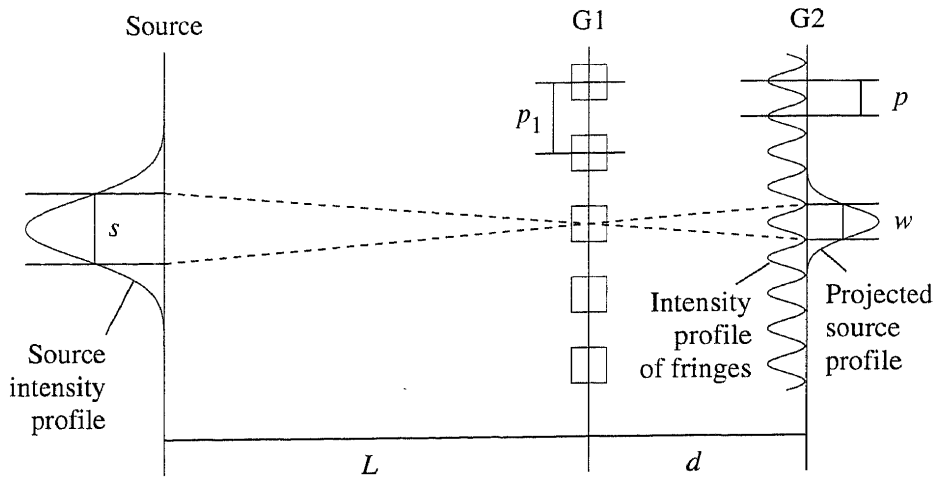

Figure 3: Setup of a two-grating interferometer with a single source spot of finite size s. The beam-splitter grating G1, with pitch p_1, is placed at a distance L from the source. At a distance d downstream of G1, each point in the source creates a set of linear fringes of period p. These fringes are washed out by the non-zero source size, i. e., by the imperfect spatial coherence of the beam illuminating G1. The resulting fringe intensity profile is the point-source profile convoluted with the projected source profile of width $w = sd/L$. (For simplicity, the analyzer grating G2, with a pitch $p_2 = p$, is not shown in this sketch.)

In this paper we discuss in some more detail the requirements on spatial coherence. We assume that the interferometer as shown in Fig. 1 is illuminated by a chaotic source with a Gaussian intensity profile, as sketched in Fig. 3. Let s denote the full width at half maximum value (FWHM) of the source intensity profile taken along the direction perpendicular to the lines of the interferometer gratings. Let us further assume that the beam-splitter grating G1 is located at a distance L from the source, and the analyzer grating G2 at a distance d downstream of the beam splitter. (For simplicity, we assume that the detector is located just behind the analyzer, so the analyzer position coincides with the detector plane.) Figure 3 illustrates the setup. We also restrict our considerations to the case of a quasi-plane wave, so that the scaling factors for a spherical wave (Eqs. 5, 6) can be neglected.

The intensity before the analyzer is a fringe pattern generated by the beam splitter. Neglecting higher diffraction orders, this fringe pattern can be approximated as a sinusoidal intensity profile.

Furthermore, if the inter-grating distance d is chosen to be one of the Talbot distances at which the contrast takes its maximum, the minima of the intensity profile are zero (if the source is infinitesimally small). The fringe profile for completely coherent illumination can then be expressed as

$$I(x) = I_0(1 + \sin(2\pi x/p_2)),$$ (9)

where x is the transverse coordinate perpendicular to the grating lines, I_0 the intensity incident on the beam splitter, and p_2 the period of the fringes.

But in the case of a source of finite size s, i. e., with only partially coherent illumination, the intensity profile observed is a convolution of the profile from a point source with the projected source profile. With the assumption of a Gaussian-shaped source, this means a convolution with a Gaussian of width

$$w = sd/L,$$ (10)

where we take both s and w to represent the full width at half maximum (FWHM) of the Gaussians. We will refer to w as the *projected source size*.

As a result, the *visibility* V of the finges, which is unity in the case of a point source, is reduced. The visibility is defined as $V = (I_{max} - I_{min})/(I_{max} + I_{min})$, where I_{max} and I_{max} are the maximum and, respectively, minimum values of intensity
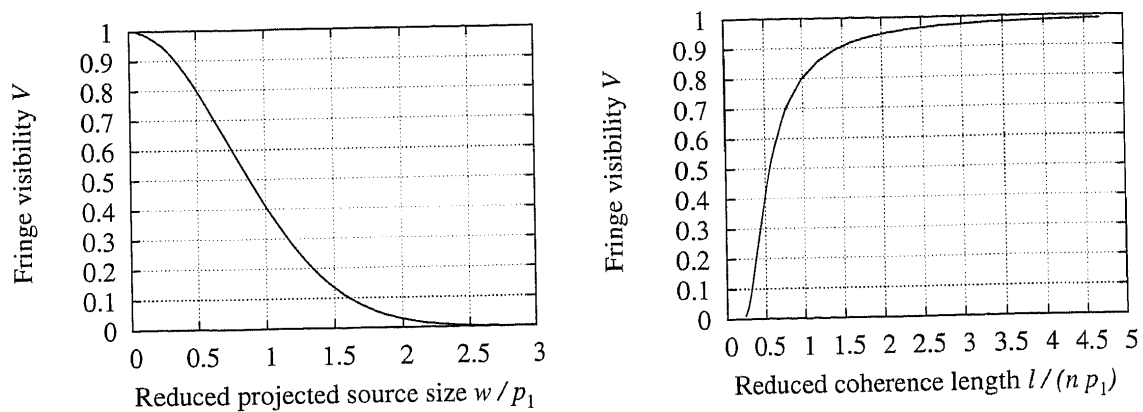
Figure 4: Visibility of a sinusoidal fringe pattern as a function of projected source size w (*left*, in units of beam-splitter grating period p_1) and as a function of the reduced transverse coherence length $l_c/(np_1)$ (*right*). The projected source size w is expressed as the full width at half maximum (FWHM), and the coherence length is defined so that $l_c = \lambda/\alpha$, with λ the X-ray wavelength and α the angular FWHM source size.

of the sinusoidal fringe pattern

$$I(x) = \frac{(I_{\max} + I_{\min})}{2} + \frac{(I_{\max} - I_{\min})}{2} \sin(2\pi x/p_2) . \tag{11}$$

The decrease of visibility with increasing projected source size w follows the relation

$$V = e^{-(1.887\, w/p_2)^2} , \tag{12}$$

i. e., the visibility decrease as a function of increasing source size has a Gaussian profile (Fig. 4, left plot). (Equation 12 follows simply from an analytical or numerical investigation of the properties of the convolution of a sine with a Gaussian profile.)

Thus, for a given required minimum visibility V_0, it follows directly from Equation 12 that the width w of the projected source profile should be

$$w \leq 0.53\sqrt{\ln V_0} . \tag{13}$$

Now the projected source size w, introduced in Eq. 10, can be expressed in terms of the Talbot order n by substituting Eq. 1 in Eq. 10:

$$w = s \times \frac{np_2^2}{2\lambda L} \tag{14}$$

For the coherence length, there are various concurrent definitions commonly in use that differ by a constant factor. We define the spatial, or transverse, coherence length l_c so that

$$l_c = \frac{\lambda L}{s} . \tag{15}$$

Substituting this into Eq. 14 yields

$$\frac{w}{p_2} = \frac{np_2}{2l_c} . \tag{16}$$

The visibility as a function of coherence length l_c is then obtained by substituting Eq. 16 into Eq. 12:

$$V = e^{-(0.94\, np_2/l_c)^2} . \tag{17}$$

The plot on the right in Fig. 4 shows this relation, which also obviously implies that the coherence length required to obtain a given visibility V_0 is

$$l_c \geq 0.94\, np_2\, (\ln V_0)^{-1/2} . \tag{18}$$

4. THE TALBOT–LAU INTERFEROMETER

The coherence requirements derived above can easily be met at modern synchrotron radiation sources, but fulfilling them with standard X-ray laboratory (or hospital) sources is a challenge since reasonable flux must be maintained at the same time. Figure 5 illustrates this: it shows a comparison of fringe patterns under coherence conditions typical of a synchrotron source and, respectively, an X-ray tube. The results for the X-ray tube parameter set makes it evident that any efficient operation of a grating interferometer at an X-ray tube source requires a modification of the experimental setup.
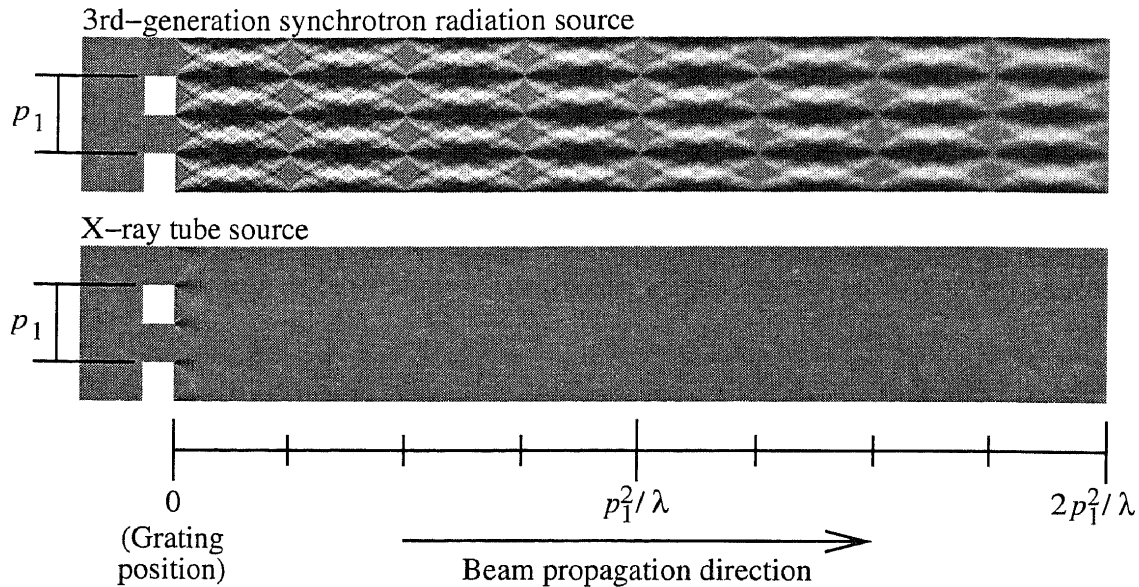
3rd–generation synchrotron radiation source

X–ray tube source

0
(Grating position)

p_1^2/λ

$2p_1^2/\lambda$

Beam propagation direction

Figure 5: Calculated intensity distribution behind a beam-splitter phase grating, for different conditions of spatial coherence. The illuminating wave has a photon energy of 14.4 keV; the beam splitter has a pitch of $p_1 = 4$ μm and its lines shift the phase by π. *Top:* conditions typical of a third-generation synchrotron source: transverse coherence length $l_c = 70$ μm, corresponding to a source of 50 μm size at 40 m distance. *Bottom:* conditions typical of a standard X-ray tube source: coherence length 0.7 μm, as would be the case for a line source of 0.25 mm transverse size located 2 m from the beam splitter.
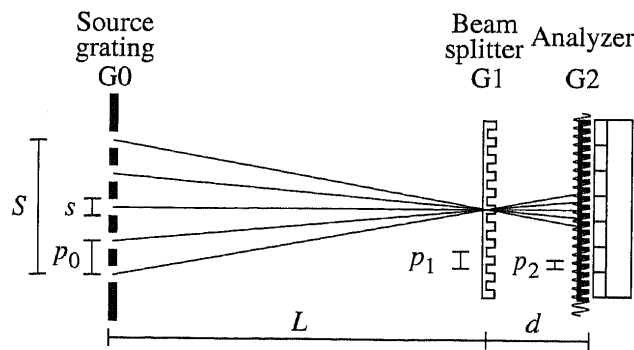
Figure 6: Setup of a Talbot–Lau interferometer using an amplitude grating G0 to create an array of equidistant virtual sources.

The additional feature that allows to greatly ameliorate the efficiency of a grating interferometer when it is used with a chaotic radiation source of large size is to structure the source and partition it into a set of equidistant smaller sources.[11]

Among the conceivable schemes to do this, the easiest to introduce into an existing setup with a standard X-ray tube is to introduce yet another amplitude grating G0 to the setup, just behind the source (Fig. 6). This grating acts as a set of slit apertures, in which each aperture makes a virtual source.

In this setup, which is known in matter-wave interferometry as a Talbot–Lau interferometer,[12,13] the different virtual sources are mutually incoherent, but each of them is small enough to create a fringe pattern with good visibility in the
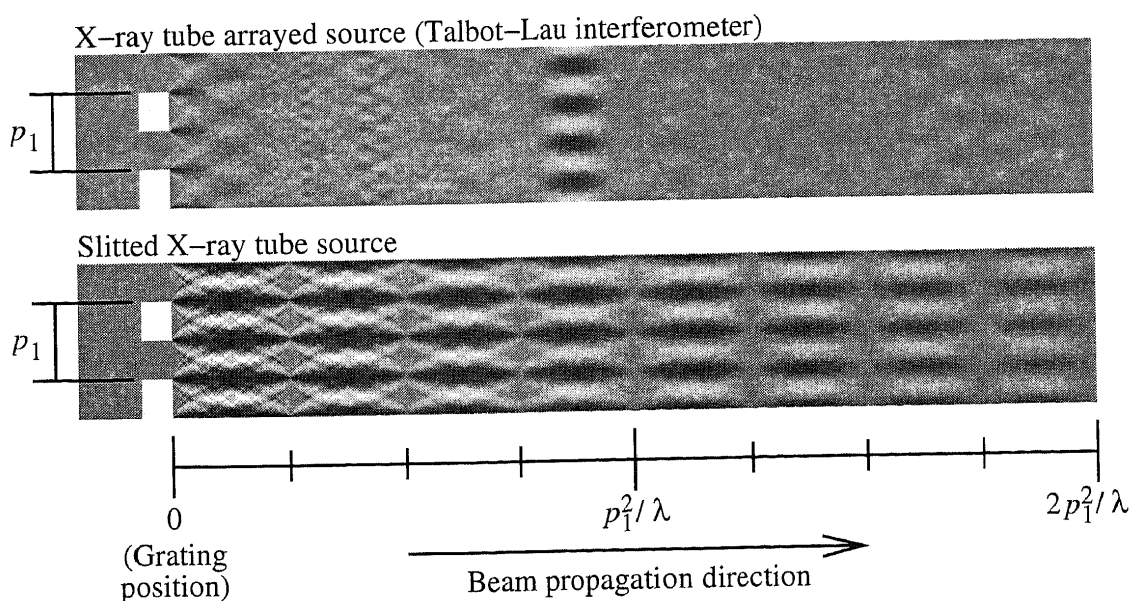
X-ray tube arrayed source (Talbot-Lau interferometer)

Slitted X-ray tube source

p_1

p_1

0
(Grating
position)

p_1^2/λ

$2p_1^2/\lambda$

Beam propagation direction

Figure 7: *Top:* Intensity distribution calculated for the same conditions as the bottom panel of Fig. 5 (typical of an X-ray tube), but assuming an arrayed source, here 10 line sources of 6.15 μm width each on an equidistant linear grid of 24.6 μm pitch, located $L = 2$ m from the beam splitter grating. The entire transverse size of the source, 10×24.6 μm $= 0.25$ mm, is the same as that of Fig. 5, bottom. The source grid spacing and distance L have been matched to enhance fringe visibility in the 7th Talbot order, i. e., at $D_7 = (7/8)p_1^2/\lambda$. *Bottom:* Intensity distribution assuming a single source of size 6.15 μm instead of the array of sources in the upper panel.

analyzer plane. Although the fringe patterns from the virtual sources add up incoherently in the analyzer plane, this incoherent addition is constructive if the spacing of the virtual sources is properly chosen. This is the case if the fringe patterns of neighboring virtual sources are displaced by exactly one fringe period (or multiples thereof) with respect to each other. This condition is fulfilled if the pitch of G0 is

$$p_0 = \frac{d}{L}\, p_2 \,.$$

(19)

Figure 7 (top) shows how a source grating designed for the 7th Talbot distance, D_7, works. For this calculation, an opening width of 6.15 μm and a spacing of 24.6 μm between adjacent openings (center-to-center) was assumed. The bottom panel of Fig. 7 gives a comparison with a single slit of the same width (but many times less intensity, which is not visible in the calculation, since it did not take counting statistics into account). As can be seen from Fig. 8, the visibility for the arrayed sources is as good as that of the single slit, but the signal is increased by a factor equal to the number of virtual sources.

Thus, in a Talbot-Lau interferometer, the effective coherence length determining the visibility of the fringes is given by the size of the individual virtual sources, not by the total size of the source. In this way, the Talbot-Lau interferometer allows an efficient implementation of phase-contrast imaging into instruments based on low-brilliance sources.

It is instructive to note that the Talbot-Lau geometry decouples the relevant properties of transverse coherence of the illuminating radiation from the total source size. The *spatial resolution* of the images, however, is determined by the total source size and the distances between source and sample and between sample and detector in exactly the same way as for a non-interferometric imaging system. The Talbot-Lau interferometry does not enhance spatial resolution in any way, but it gives phase sensitivity where it would otherwise not be accessible.

Figure 9 shows an experimental result obtained using this principle: a pair of absorption and differential-phase radiographs obtained with a standard sealed-tube laboratory X-ray tube and a Talbot-Lau interferometer. Other results have been published elsewhere.[14] For the results shown here, the design energy of the interferometer setup was 28 keV. The experiments were carried out on a Seifert ID 3000 x-ray generator operated at 35 kV / 30 mA. We used a tungsten line focus tube (DX-W8x0.4-L) with a focus size of 8×0.4 mm² (horizontal $\times$ vertical). Due to the inclination of the target with respect to the optical axis of our setup of $6°$, the effective source size was 0.8×0.4 mm². The gratings were fabricated by a
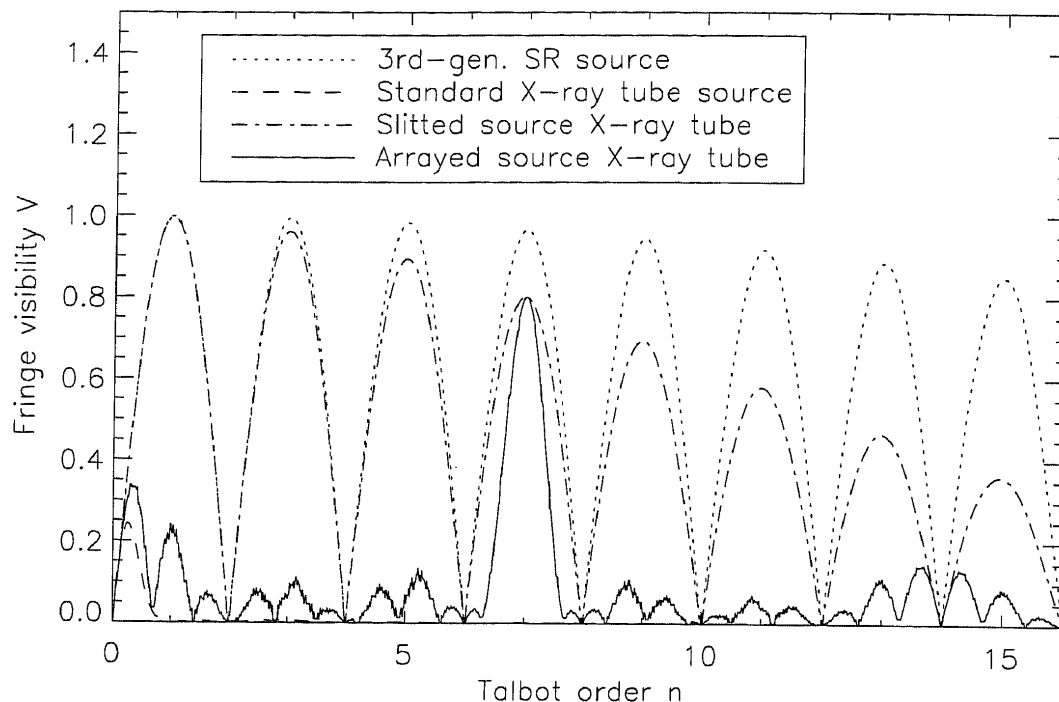
Figure 8: Visibility V of the 2-μm-period fringes from the intensity distributions shown in Figs. 5 and 7, as a function of distance downstream of the grating. The distance is expressed in terms of the Talbot order n, corresponding to a distance $D_n = (n/8)p_1^2/\lambda$.

process involving photolithography, deep etching into silicon[15, 16] and electroplating of gold. They were placed with their lines perpendicular to the optical axis of the setup. They had periods of $p_0 = 73\ \mu$m, $p_1 = 3.9\ \mu$m, $p_2 = 2.0\ \mu$m. The depth of the grating structures were 42 μm (G0), 35 μm (G1), and 26 μm (G2). The distances between the gratings were $L = 1.57$ m and $d = 43$ mm. The images were recorded using a 150-μm-thick caesium iodide (CsI) scintillation screen with a demagnifying optical lens system and a cooled charge coupled device (CCD: Fingerlakes Instruments, FLI IMG
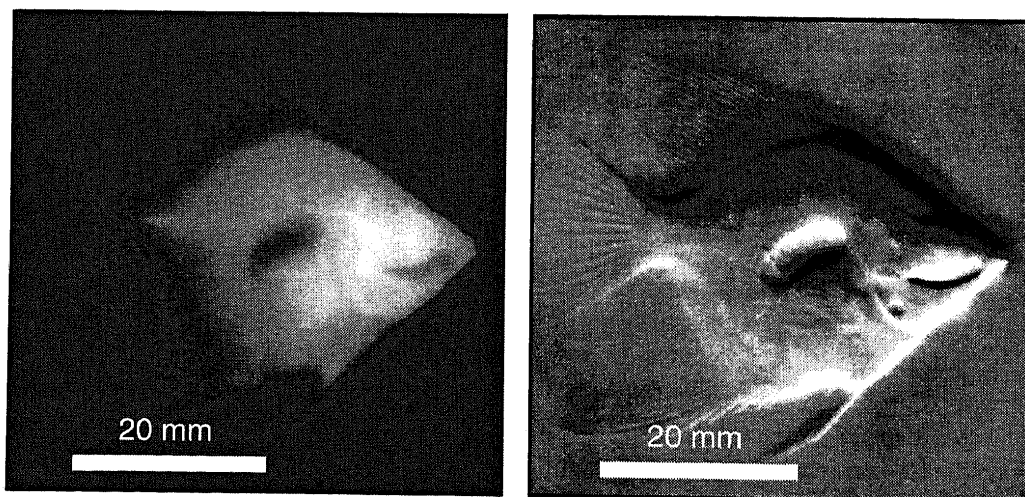

Figure 9: Absorption *(left)* and differential phase contrast image *(right)* of a fish, taken with a Talbot–Lau interferometer. The images are extracted from the same phase-stepping scan.

1001, KODAK chip with 1024×1024 pixels, $(24 \ \mu\text{m})^2$ pixel size). The effective spatial resolution was mainly determined by the thickness of the scintillation screen to ≈ 0.1 mm. The size of the gratings, and thus the field of view, is currently limited to $64 \times 64 \ \text{mm}^2$ by the 100-mm-wafer processing technology, but there are no principle constraints hindering the upscaling by using state-of-the-art (300-mm-wafer) techniques.

5. CONCLUSIONS AND OUTLOOK

A Talbot grating interferometer can be used efficiently with polychromatic radiation from a standard, sealed-tube X-ray laboratory source if the setup is extended to a Talbot–Lau interferometer by the use of an additional amplitude grating, placed between the source and the sample and creating a set of equidistant virtual source points. The theoretical considerations in this paper complement the experimental demonstration of this principle reported earlier this year.[14] The principle can also be applied to other types of radiation where sources of high brilliance are not available, such as neutrons.[17] In X-ray imaging, the Talbot–Lau interferometer may help extend the use of phase contrast beyond the limited range of applications given by the obligation to use a synchrotron-radiation source or a microfocus X-ray tube.

6. ACKNOWLEDGMENTS

REFERENCES

1. C. David, B. Nöhammer, H. H. Solak, and E. Ziegler, "Differential x-ray phase contrast imaging using a shearing interferometer," *Appl. Phys. Lett.* **81**, pp. 3287–3289, 2002.
2. A. Momose, "Demonstration of X-ray Talbot interferometry," *Jpn. J. Appl. Phys.* **42**, pp. L866–L868, 2003.
3. T. Weitkamp, A. Diaz, B. Nöhammer, F. Pfeiffer, T. Rohbeck, P. Cloetens, M. Stampanoni, and C. David, "Hard X-ray phase imaging and tomography with a grating interferometer," in Bonse,[18] pp. 137–142.
4. A. Momose, S. Kawamoto, I. Koyama, and Y. Suzuki, "Phase Tomography Using an X-ray Talbot Interferometer," in Bonse,[18] pp. 352–360.
5. T. Weitkamp, A. Diaz, B. Nöhammer, F. Pfeiffer, M. Stampanoni, E. Ziegler, and C. David, "Moiré interferometry formulas for hard X-ray wavefront sensing," in *Advances in Mirror Technology for X-Ray, EUV Lithography, Laser, and Other Applications II*, A. M. Khounsary, U. Dinger, and K. Ota, eds., *Proceedings SPIE* **5533**, pp. 140–144, SPIE, (Bellingham, WA), 2004.
6. T. Weitkamp, B. Nöhammer, A. Diaz, C. David, and E. Ziegler, "X-ray wavefront analysis and optics characterization with a grating interferometer," *Appl. Phys. Lett.* **86**, p. 054101, 2005.
7. T. Weitkamp, A. Diaz, C. David, F. Pfeiffer, M. Stampanoni, P. Cloetens, and E. Ziegler, "X-ray phase imaging with a grating interferometer," *Optics Express* **13**, pp. 6296–6304, 2005.
8. F. Pfeiffer, O. Bunk, C. Schulze-Briese, A. Diaz, T. Weitkamp, C. David, J. F. van der Veen, I. Vartanyants, and I. K. Robinson, "Shearing interferometer for quantifying the coherence of hard X-ray beams," *Phys. Rev. Lett.* **94**, p. 164801, 2005.
9. C. David, T. Weitkamp, T. Khan, F. Pfeiffer, O. Bunk, A. Diaz, T. Rohbeck, A. Groso, and M. Stampanoni, "Quantitative phase imaging and tomography with polychromatic X rays," in *Proceedings of The 8th International Conference on X-ray Microscopy (XRM2005), 26–30 July 2005, Himeji, Japan, IPAP Conference Series* **7**, pp. 346–348, Insitute of Pure And Applied Physics (Japan), 2006.
10. A. Momose, W. Yashiro, Y. Takeda, Y. Suzuki, and T. Hattori, "Phase tomography by X-ray Talbot interferometry for biological imaging," *Jpn. J. Appl. Phys.* **45**, pp. 5254–5262, 2006.
11. C. David, F. Pfeiffer, and T. Weitkamp, "Interferometer for quantitative phase contrast imaging and tomography with an incoherent polychromatic x-ray source." European patent application no. EP05012121, received 6 June 2005.
12. J. F. Clauser and S. F. Li, "Heisenberg microscope decoherence atom interferometry," *Phys. Rev. A* **50**, pp. 2430–2433, 1994.
13. B. Brezger, L. Hackermüller, S. Uttenthaler, J. Petschinka, M. Arndt, and A. Zeilinger, "Matter-wave interferometer for large molecules," *Phys. Rev. Lett.* **88**, p. 100404, 2002.

14. F. Pfeiffer, T. Weitkamp, O. Bunk, and C. David, "Phase retrieval and differential phase-contrast imaging with low-brilliance X-ray sources," *Nature Physics* **2**, pp. 258–261, 2006.

15. C. David, B. Nöhammer, and E. Ziegler, "Wavelength tunable diffractive transmission lens for hard x rays," *Appl. Phys. Lett.* **79**, pp. 1088–1090, 2001.

16. C. David, B. Nöhammer, E. Ziegler, and O. Hignette, "Tunable diffractive optical elements for hard X rays," in *X-ray micro- and nano-focusing: applications and techniques II*, I. McNulty, ed., *Proceedings SPIE* **4499**, pp. 96–104, SPIE, (Bellingham, WA), 2001.

17. F. Pfeiffer, C. Grünzweig, O. Bunk, G. Frei, E. Lehmann, and C. David, "Neutron phase imaging and tomography," *Phys. Rev. Lett.* **96**, p. 215505, 2006.

18. U. Bonse, ed., *Developments in X-ray Tomography IV*, *Proceedings SPIE* **5535**, (Bellingham, WA), SPIE, 2004.